JBC RESEARCH ARTICLE

Structure-based interface engineering methodology in designing a thermostable amylose-forming transglucosylase

Received for publication, February 4, 2022, and in revised form, May 23, 2022 Published, Papers in Press, May 25, 2022,
https://doi.org/10.1016/j.jbc.2022.102074

Yuqing Tian[1], Xiaodong Hou[2], Dawei Ni[1], Wei Xu[1], Cuie Guang[1], Wenli Zhang[1], Qiuming Chen[1], Yijian Rao[2,*], and Wanmeng Mu[1,3,*]

From the [1]State Key Laboratory of Food Science and Technology, [2]Key Laboratory of Carbohydrate Chemistry and Biotechnology, Ministry of Education, School of Biotechnology, and [3]International Joint Laboratory on Food Safety, Jiangnan University, Wuxi, Jiangsu, China

Edited by Joseph Jez

Many drugs and prebiotics derive their activities from sugar substituents. Due to the prevalence and complexity of these biologically active compounds, enzymatic glycodiversification that facilitates easier access to these compounds can make profound contributions to the pharmaceutical, food, and feed industries. Amylosucrases (ASases) are attractive tools for glycodiversification because of their broad acceptor substrate specificity, but the lack of structural information and their poor thermostability limit their industrial applications. Herein, we reported the crystal structure of ASase from *Calidithermus timidus*, which displays a homotetrameric quaternary organization not previously observed for other ASases. We employed a workflow composed of five common strategies, including interface engineering, folding energy calculations, consensus sequence, hydrophobic effects enhancement, and B-factor analysis, to enhance the thermostability of *C. timidus* ASase. As a result, we obtained a quadruple-point mutant M31 ASase with a half-life at 65 °C increased from 22.91 h to 52.93 h, which could facilitate biosynthesis of glucans with a degree of polymerization of more than 20 using sucrose as a substrate at 50 °C. In conclusion, this study provides a structural basis for understanding the multifunctional biocatalyst ASase and presents a powerful methodology to effectively and systematically enhance protein thermostability.

Enzymes play an indispensable role in various fields, including industrial, environmental, and biomedical technology, owing to their outstanding selectivity and regiospecificity (1). However, many industrial applications based on enzymatic or chemoenzymatic pathways are still hindered due to the lack of biocatalysts that can withstand harsh conditions (2). Among them, the most common limiting factor is the thermostability of enzymes because the reaction temperature can affect the reaction rate, solubility and viscosity of the reactants, possibility of microbial contamination, and position of the reaction equilibrium (3). Thermostability is related to the balance between protein folding and unfolding. The most direct way to increase thermostability is to create or enhance interactions between residues of the protein (4). Therefore, it attracts increasing attention to enhance the thermostability of enzymes through protein engineering.

Common strategies of protein engineering to enhance thermostability include increasing the similarity to the consensus sequence or calculating the B-factors of residues and directionally changing their flexibility (5). For multimeric enzymes, it is necessary to optimize interface interactions. Meng *et al.* (6) analyzed 172 computationally designed ω-transaminase mutants and found that 56% of interface mutations can bring thermal stabilization effects, while only 6% of surface mutations bring stabilization effects. Additionally, the hydrophobic effect plays a crucial role in protein stability (7), and the redesign of a well-packed hydrophobic core based on computational simulation has attracted considerable attention (8). The thermostability of numerous enzymes has been improved through protein engineering based on various strategies (9). However, most of these strategies require time-consuming and laborious high-throughput work. Therefore, there is still a lack of systematic, effective, and minimally invasive strategies for protein engineering to improve the thermostability of enzymes, particularly multimeric enzymes.

Carbohydrate-active enzymes refer to enzymes that catalyze the assembly, cleavage, and modification of carbohydrates (10). Among the carbohydrate-active enzymes, the glycoside hydrolases (GH) family enzymes can use cheap biomass such as sucrose and starches instead of expensive nucleotide-active sugars as donor substrates, attracting increasing attention for their cost-effective glycodiversification ability (11). Amylosucrase (ASase, EC 2.4.1.4) is a sucrose-utilizing transglucosylase belonging to the GH13 family, which can catalyze several types of reactions (Fig. 1) as polymerization, isomerization, and transglycosylation. It can recognize more than 50 substances as glycosyl acceptors, and its donor substrate, sucrose, is abundant and readily available (12). ASases have broad application potential in producing functional sweeteners, dietary fibers, carbohydrate-based carrier materials, bioactive compounds, and cell surface oligosaccharides (Fig. 1). However, of the limited number of identified ASases, most show poor

* For correspondence: Wanmeng Mu, wmmu@jiangnan.edu.cn; Yijian Rao, raoyijian@jiangnan.edu.cn.

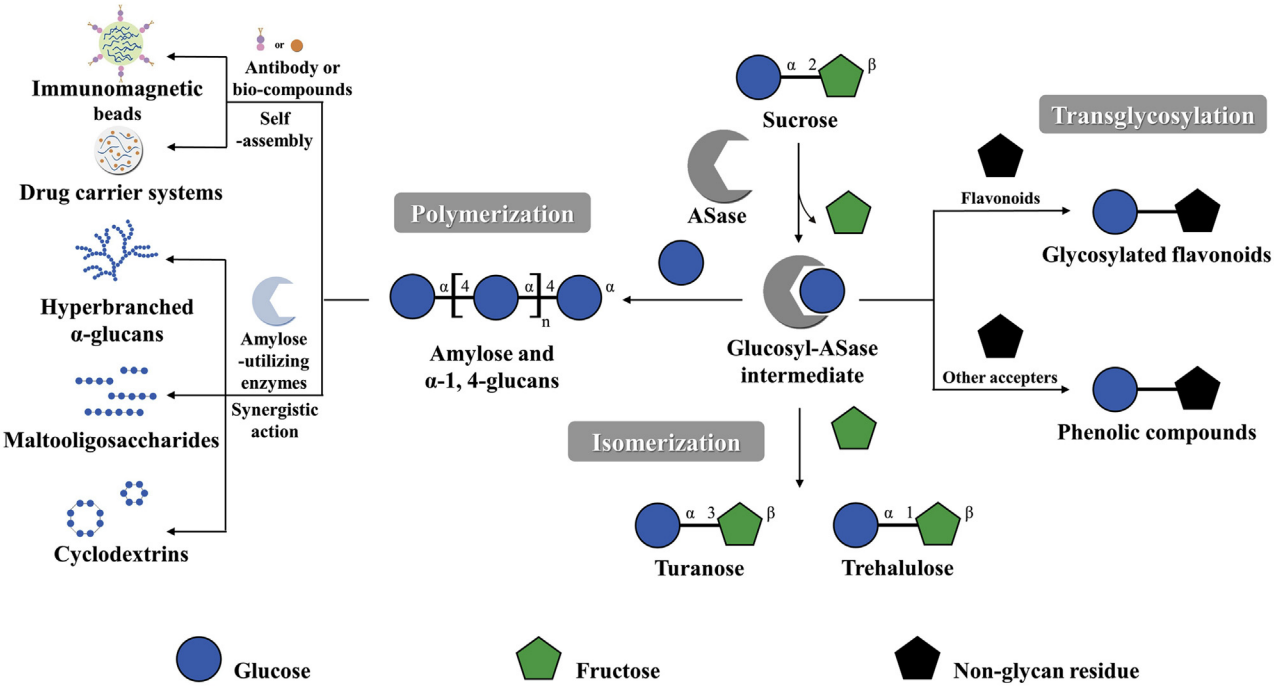

Figure 1. Reactions catalyzed by ASase and various applications limited by its thermostability.

thermostability and are very easy to inactivate even at 50 °C (13), severely limiting their industrial applications. Therefore, we have mined a novel ASase from *Calidithermus timidus* DSM 17022 (CT-ASase). CT-ASase exists as a homotetramer in solution (14), different from other reported monomeric and dimeric ASase. Although its thermostability still cannot meet industry needs to keep stable above 60 °C, its unique homotetrameric organization may become a key factor to improve its thermostability. However, due to the lack of structural information of CT-ASase, the relationship between its thermostability and tetrameric quaternary organization cannot be confirmed.

Therefore, in this study, we solved the crystal structure of CT-ASase, the first three-dimensional structure of tetrameric ASase, and investigated the impact of interface regions on its thermostability. To enhance the thermostability of CT-ASase, we constructed a structure-based workflow, which combined five strategies, including interface engineering, folding energy calculations, consensus sequence, hydrophobic effects enhancement, and B-factor analysis. Finally, a quadruple-point mutant M31 (L382P/S414N/P618I/H631R) was obtained with the half-life at 65 °C increasing from 22.91 h to 52.93 h. Molecular dynamics (MD) analyses, including binding free energy calculation, root mean square deviation (RMSD), and root mean square fluctuation (RMSF), also proved the stabilizing effect of these four mutation sites on the subunit interfaces. Furthermore, M31 possessed superior polymerization ability at 50 °C. When just adding only 0.04 U/ml of M31 at 50 °C, glucans with a degree of polymerization of more than 20 can be synthesized from sucrose, while the wildtype CT-ASase (WT) hardly catalyzes the synthesis of glucans under the same conditions.

Results

Overall structure and subunit assembly

Unlike other reported monomeric and dimeric ASase, CT-ASase existed as a homotetramer in solution (Fig. S1). Therefore, to obtain accurate structural information about the tetrameric ASase, we investigated the crystallization of CT-ASase. As shown in Table S1, the three-dimensional structure of CT-ASase was solved at a resolution of 2.29 Å (Protein Data Bank/PDB entry: 7ESH). The tetrameric CT-ASase with a buried area of 7387 Å^2 out of a total surface area of 88,342 Å^2 was observed. Each monomer had its active site and contained five domains (Figs. 2*A* and S2): domains N, A, B, B', and C. Among them, domains A, B, and C are shared in the GH13 family (15), while the other two domains are the feature domains of ASase. Domain A is the catalytic domain, which adopts a typical $(\beta/\alpha)_8$-barrel structure. Domain C, also known as the β-sandwich domain, is thought to be involved in glucan anchoring and extension with domain B' (16).

The tetrameric arrangement of CT-ASase can be referred to as a dimer of dimers. As shown in Figure 2*B*, each chain interacted with two chains in the tetramer, forming two types of interfaces. One type of interface was formed between chains A and D and chains B and C. This interface was the unique interface of tetrameric ASase, referred to as the interdimer interface. Stabilization of the interdimer interface benefited from the interaction between domains A, B', and C (Fig. 2*B*

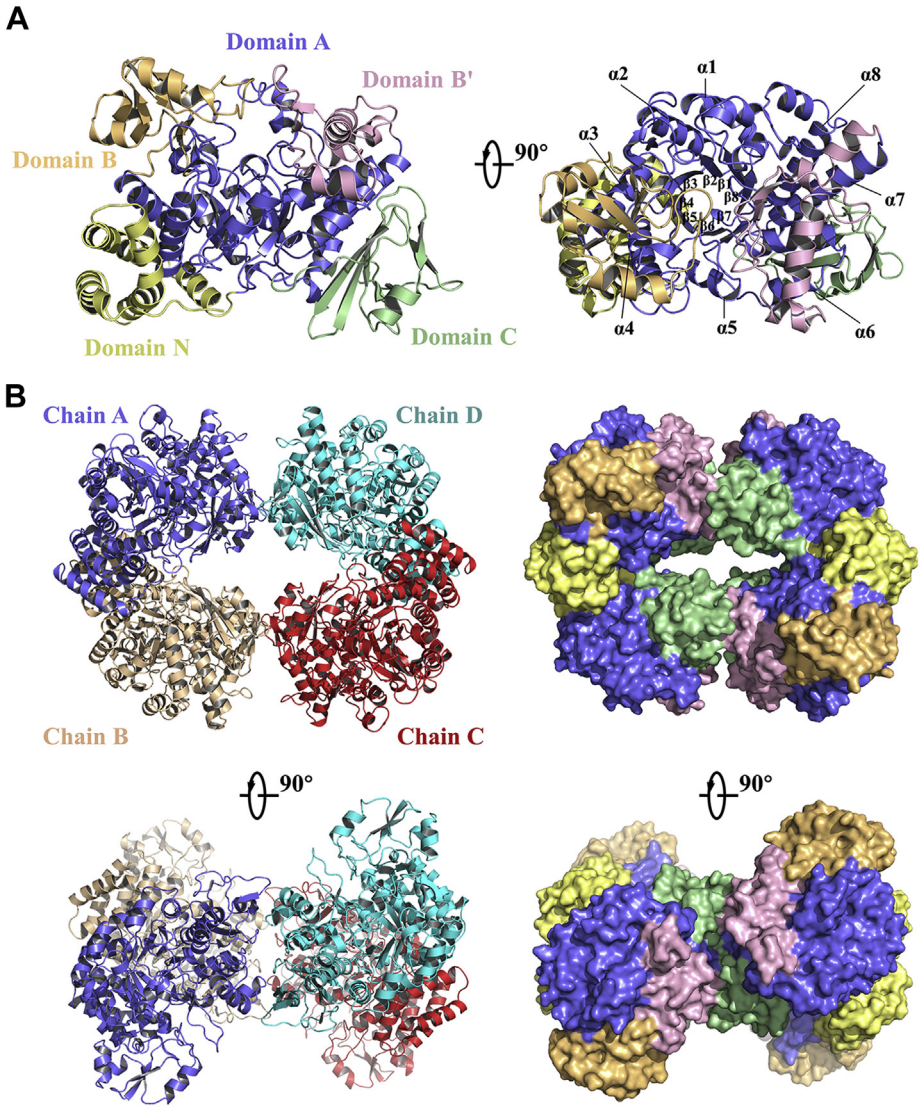

Figure 2. Graphical display of the crystal structure of CT-ASase. *A*, tertiary structure. The domains A, N, B, B′, and C are shown in *violet*, *yellow*, *orange*, *pink*, and *green*. *B*, quaternary structure. The chains A, B, C, and D are shown in *violet*, *wheat*, *red*, and *cyan*, respectively, in the cartoon representation of CT-ASase (*left*). In the surface representation of CT-ASase (*right*), five domains are displayed with the same color as (*A*) to exhibit the domains involved in the intersubunit interaction. CT-ASase, amylosucrase from Calidithermus timidus DSM 17022.

right). Another type of interface was formed between chains A and B and chains C and D, which had a similar pattern to dimeric DG-ASase (ASase from *Deinococcus geothermalis*) and DRd-ASase (ASase from *Deinococcus radiodurans*) and thereby could be referred to as an intradimer interface. Stabilization of the intradimer interface benefited from the interaction between domains N, A, and C (Fig. 2*B* right).

Insights into subunit interface

To decode this novel subunit arrangement mode, we analyzed the intersubunit interaction of the two different subunit interfaces of CT-ASase. The interdimer interface was the unique interface of tetrameric ASase. It exhibited an average buried area of 611.9 Å^2 per subunit and was composed of five regions that widely participated in hydrophobic interactions (Fig. S3). In addition to hydrophobic interactions, a dense network of hydrogen-bonding interactions was also observed between residues Arg371, Arg410, Gly412, Arg576, and Asn577 (Fig. 3*A*). The interdimer interface exhibited a shape complementarity. H19 and H20 belonging to domain B' of one subunit fitted into the shallow groove formed by H30, S21, and S24 of domain C of another subunit (Fig. 3*B*). Two loops were also involved in interdimer interactions, including the loop between H19 and H20 of domain B' and the loop connecting S18 and S19 of domain C.

The intradimer interface of tetrameric CT-ASase exhibited a moderate average buried area of 1235 Å^2 per subunit, which was 240 Å^2 less than that of DG-ASase, and 192 Å^2 more than that of DRd-ASase. A salt bridge was formed between Glu31 and Arg79, similar to the salt bridge formed between Glu25 and Arg74 in DG-ASase (17). Another salt bridge was formed between Glu38 and Lys83, different from DG-ASase and DRd-ASase. Like dimeric DG-ASase and DRd-ASase, tetrameric

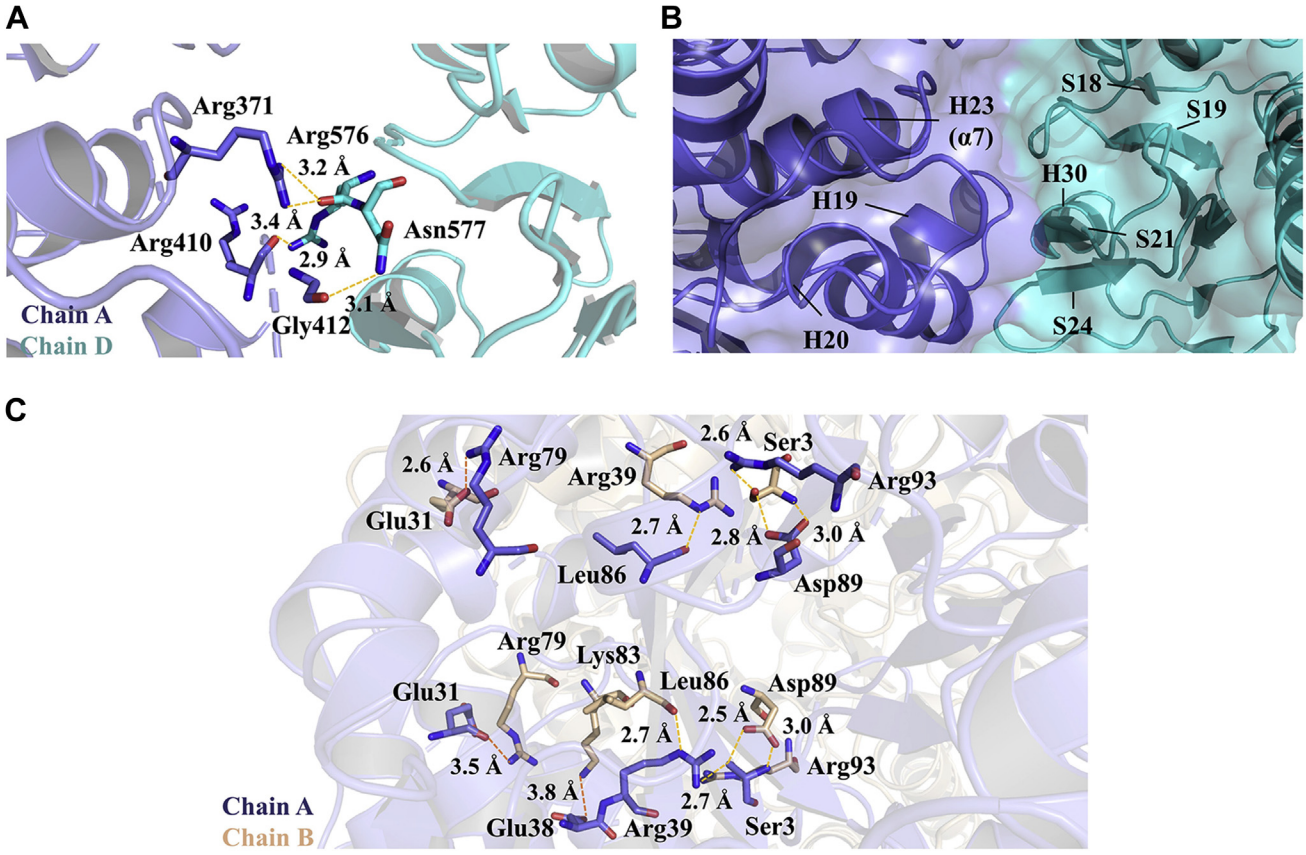

Figure 3. Subunit interface interaction network of CT-ASase. *A*, hydrogen bonds involved in forming the interdimer interface. *B*, secondary structural elements involved in forming the interdimer interface. *C*, hydrogen bonds and salt bridges involved in forming the intradimer interface. The same color code is used throughout the different views: chain A (*violet*), chain B (*red*), and chain D (*cyan*). Hydrogen bonds are represented by *yellow dashed lines*, and salt bridges are represented by *orange dashed lines*. Helixes are abbreviated as H and numbered, and strands are abbreviated as S and numbered. α1–α8 refer to the α-helixes belonging to the (β/α)8-barrel structure. CT-ASase, amylosucrase from *Calidithermus timidus* DSM 17022.

CT-ASase also had two insertion regions located at the intradimer interface. These two regions were Gly342–Gly346 and Pro588–Gly590, five and four residues longer than monomeric NP-ASase (ASase from *Neisseria polysaccharea*), respectively (Figs. 3*C* and S3). The residues Gly342–Gly346 belonged to the loop that connected the α5 and β6 of the catalytic domain and interacted with the residues Pro588–Gly590 of another subunit through extensive hydrophobic interactions, which may stabilize CT-ASase.

Probing the impact of interface regions on thermostability

Although the dimer structures of ASase were reported approximately 10 years ago, molecular modification has never focused on the subunit interface of ASases. Therefore, this study attempted to probe the impact of two types of interface regions on the thermostability of CT-ASase (Table 1).

First, we focused on the intradimer interface. Several mutants were designed to investigate the relationship between two insert regions and thermostability. M3 replaced regions 4 and 7 of the tetrameric CT-ASase with the corresponding regions of the monomeric NP-ASase, and M4 removed the two insert regions of CT-ASase. M3 and M4 showed a decrease of 14.79 °C and 11.89 °C in T_m (melting temperature), respectively. M5 and M6 were designed based on five additional residues in region 4 of dimeric DG-ASase and showed a decrease of 5.44 °C and 1.41 °C in T_m, respectively.

Then, we focused on the interdimer interface. As mentioned, the intradimer interface had two insert loop regions, which were considered characteristic of the interface regions. However, the interdimer interface did not exhibit similar characteristics. Therefore, we investigated the interdimer residues that formed hydrogen bonds. By performing alanine scanning on all residues involved in hydrogen bond interactions, we obtained the mutant R371A-R410A-G412A-R576A-N577A with T_m value reduced by 5.5 °C. Subsequently, individual alanine scanning was performed on these five residues, and their T_m values were reduced by approximately 2 °C. Among them, R410A had the highest ΔT_m of –0.5 °C; N577A had the lowest ΔT_m, which was –2.15 °C, revealing it may play a relatively important role in thermostability. Therefore, we tried to strengthen the interactions at this position and constructed mutants N577D and N577R. However, their T_m values were also reduced by about 2 °C, indicating that only optimizing residue 577 is hard to improve the thermostability of this tetramer and more effective methods such as computer-aided rational design are needed.

Table 1
Impact of interface residues on the thermostability of CT-ASase

Abbreviation	Interface region	Residue positions	Wildtype	Mutant	ΔT_m (°C)	Relative activity (%)
M3	4/6	335–346/586–591	LIHYLGQGPHFG/RHPLGN	VVQYIGQ/NNA	−14.79[a]	56.4 ± 1.3
M4	4/6	341–347/587–592	QGPHFGL/HPLGNL	QL/HL	−11.89[a]	58.8 ± 1.2
M5	4	342	G	R	−5.44[a]	72.3 ± 1.0
M6	4	342–343	GP	RA	−1.41[a]	79.5 ± 1.4
M7	4/6	345/588	F/P	C/C	−1.15[b]	79.9 ± 0.7
M8	1′/2′/2′/3′/3′	371/410/412/576/577	R/R/G/R/N	A/A/A/A/A	−5.5[b]	92.1 ± 1.8
M9	1′	371	R	A	−1.33[b]	122.8 ± 0.5
M10	2′	410	R	A	−0.51[b]	93.0 ± 1.3
M11	2′	412	G	A	−2.00[b]	76.2 ± 2.2
M12	3′	576	R	A	−1.16[b]	97.6 ± 0.7
M13	3′	577	N	A	−2.15[b]	107.6 ± 1.2
M14	3′	577	N	R	−2.05[b]	105.7 ± 1.1
M15	3′	577	N	D	−1.55[b]	117.7 ± 0.6

Abbreviation: DSC, differential scanning calorimetry.
[a] These data were estimated using DSC.
[b] These data were estimated using DSF. The consistency of ΔT_m value measured by DSC and DSF were confirmed (Table S2).

Computer-aided rational design to enhance the thermostability

To systematically and effectively enhance the thermostability of tetrameric CT-ASase, we adopted a three-step workflow, including the rational design based on five engineering strategies (Fig. 4*A*), the screening of thermal shift using the DSF (differential scanning fluorimetry) method (Fig. 4*B*), and the accumulation of sense mutations (Fig. 4*C*).

To find potentially stabilizing mutations, we first paid particular attention to the interface residues, which often have a considerable contribution to the stabilization of multimeric enzymes (4, 6, 18). Considering that the dense interaction network of the subunit interface had a great impact on the thermostability of CT-ASase, it may be challenging to improve thermostability by mutating residues naturally involved in the interface interactions. Therefore, we focused on the interface residues that do not form salt bridges or hydrogen bonds. H631R, S414N, and H632G were selected based on this strategy and three supporting strategies, including folding energy calculations, consensus sequence, and B-factor analysis.

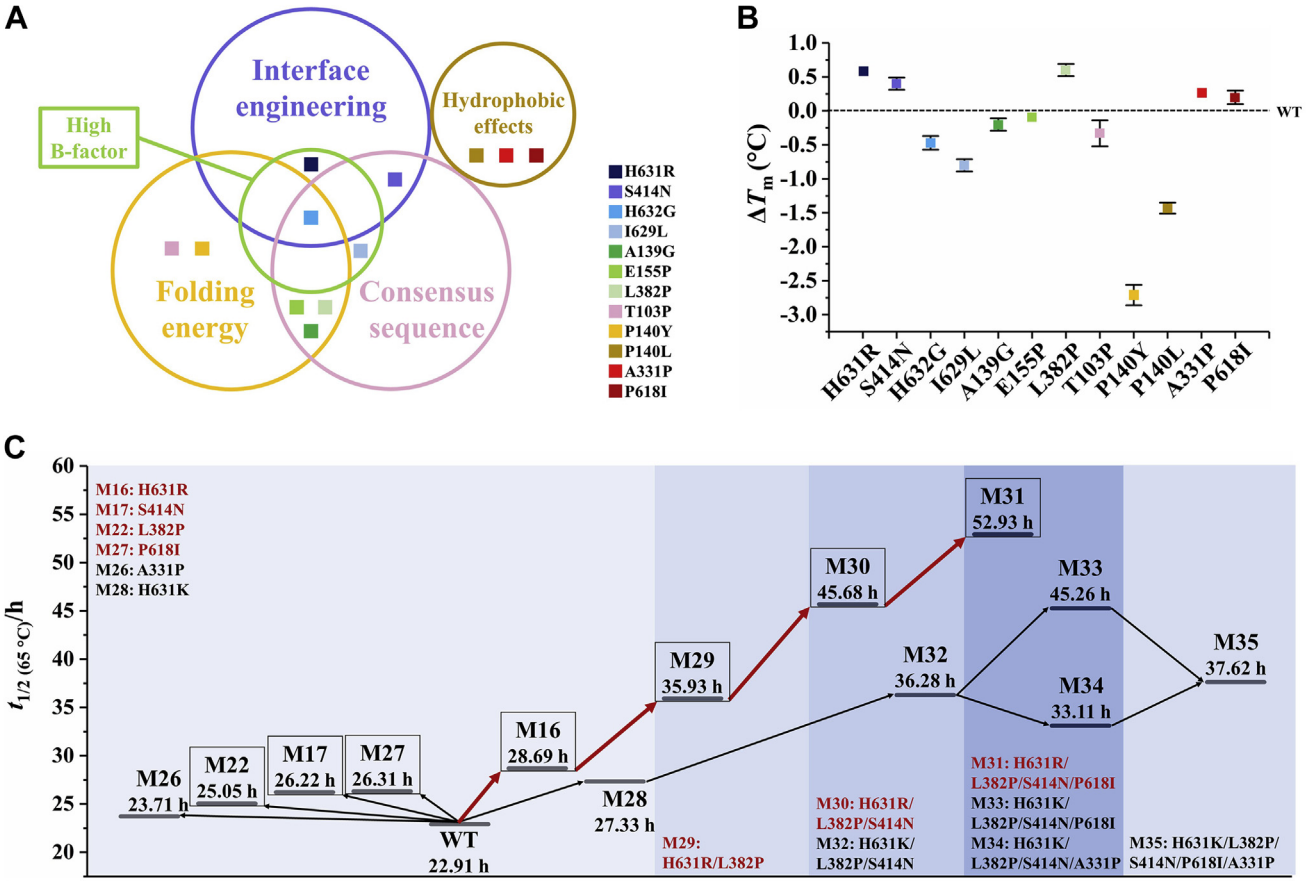

Figure 4. The workflow of the molecular modification performed in this study. *A*, twelve potentially stabilizing mutations selected by five protein engineering strategies. Five strategies and 12 mutants are shown in *circles* and *squares*. *B*, the thermal shift between wildtype CT-ASase and its variants. Error bars represent standard deviation. *C*, combination of mutations in different ways. The best combination route is shown as *orange*. ASase, amylosucrase.

Then, two and three mutants were selected based on folding energy calculations and hydrophobic effects enhancement, respectively. Folding energy calculations can predict the shift in the balance between protein folding and unfolding (9). Hydrophobic effects are crucial to protein folding, and a well-packed hydrophobic core has always been the goal of protein engineering (19–21). Next, four mutants were selected by the intersection of all five strategies. Finally, a total of 12 candidate mutants were selected for biochemical verification.

Structural analysis of the single-point mutants

Five mutants displayed enhanced T_m values among the 12 mutants selected in the previous step (Fig. 4*B* and Table S3), including A331P, L382P, S414N, P618I, and H631R.

S414N was located at the region 2' of the interdimer interface, and H631R was located at the region 5' of the interdimer interface. S414N displayed an increase of 3.31 h in half-life ($t_{1/2}$). As analyzed by LigPlot, substitution at position 414 from serine to asparagine strengthened hydrophobic contacts at the interdimer interface, which may bring the loop region of chain A (B/C/D) closer to the shallow groove of chain D (C/B/A) (Fig. 5*A*). Based on the homology analysis of 1028 similar sequences, 28.21% of the proteins had asparagine at this position, and some ASases also had asparagine at this position, such as DG-ASase, and ASases from *Alteromonas macleodii* and *Arthrobacter chlorophenolicus*. H631R had the highest $\Delta t_{1/2(65\ ^\circ C)}$ among these single-point mutants, which was 5.78 h. The residue H631 showed a high B-factor, ranking 18 out of 656 residues. Analysis of H631R using LigPlot showed that two new hydrogen bonds were formed between Arg631 of chain A (B/C/D) and Glu416 of chain D (C/B/A) (Fig. 5*B*).

L382P, P618I, and A331P were located on the surface close to the interface. L382P (Fig. 5*A*) displayed an increase of 2.14 h in $t_{1/2(65\ ^\circ C)}$. Residue 382 was located very close to the intradimer interface region 5. Analysis of 1028 similar sequences showed that 28.97% of the proteins had proline at this position, including some ASases, such as DG-ASase, DRd-ASase, and ASase from *D. radiopugnans*, and only 0.93% of the proteins had serine. Proline adopts limited configurations and can limit the configuration of surrounding residues, making the protein less easy to unfold. Therefore, high proline content in the loop is also a known feature of hyperthermophilic proteins (22). P618I displayed an increase of 3.40 h in $t_{1/2(65\ ^\circ C)}$. The residue 618 was located close to the interdimer interface region 4'. Isoleucine has a flexible side chain that can adopt four conformations (22). This conformational flexibility allows isoleucine to fill in various voids generated during the protein core packing process (Fig. 5*B*). However, these single-point mutants only had a $\Delta t_{1/2(65\ ^\circ C)}$ of up to 5.78 h, which cannot meet industrial needs. Therefore, we attempted to combine these mutations.

Combinatorial mutations to obtain hyperstable mutant

Mutation accumulation is a common strategy for obtaining stable variants, and thus, we rationally combined stabilizing single-point mutations based on the ΔT_m values. Among five single-point mutations selected in the previous step, A331P was excluded from combinatorial mutation since its antagonistic effect on kinetic stability was evident (Fig. 4*C*), which

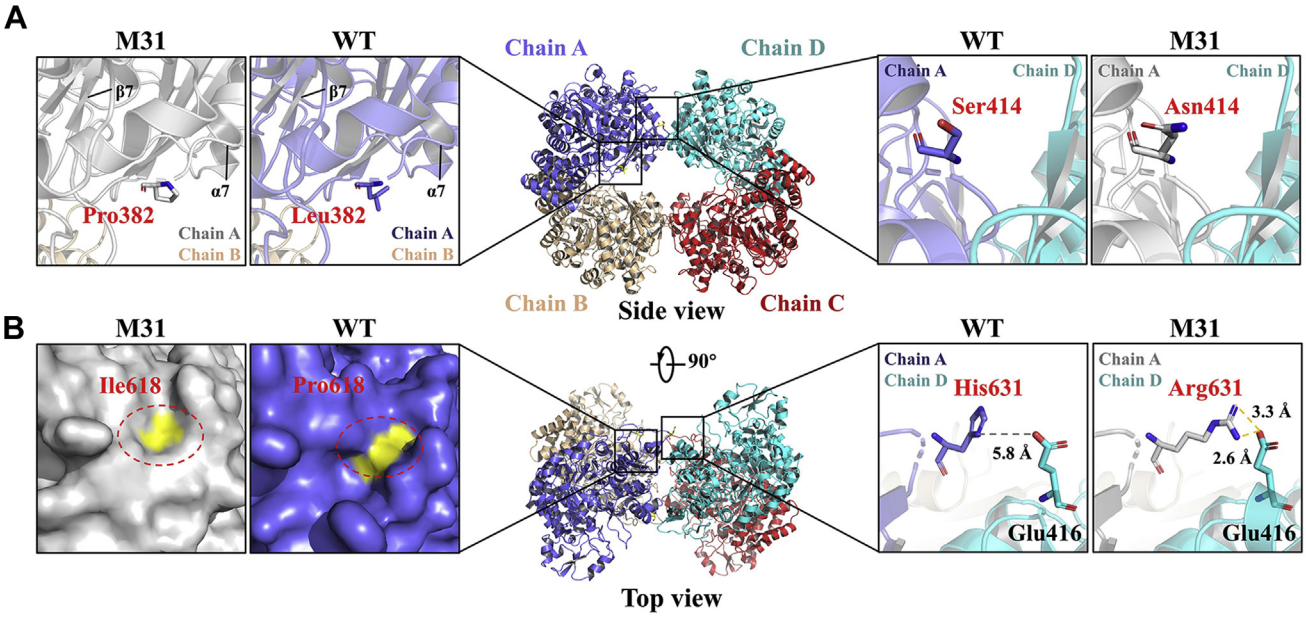

Figure 5. Structural analysis of the mutations. *A*, L382P and S414N. Proline in the loop could limit the configuration of surrounding residues and make the protein less easy to unfold. S414N brought the loop region of chain A (B/C/D) closer to the shallow groove of chain D (C/B/A). *B*, P618I and H631R. As shown by the *red dashed circle*, the conformational flexibility of isoleucine allowed it to better fill in voids generated during the protein core packing process. Two new intersubunit hydrogen bonds were formed between Arg631 of chain A (B/C/D) and Glu416 of chain D (C/B/A). All mutation sites are displayed with residues on chain A. The chain A of WT CT-ASase is shown in *violet*, while that of the mutant is shown in *gray*. The chains B, C, and D are shown in *wheat*, *red*, and *cyan*. α1–α8 specifically refer to the α-helixes belonging to the (β/α)8-barrel structure. ASase, amylosucrase.

may be due to the residue 331 being located in the catalytic domain. Furthermore, considering that lysine and arginine share similar properties, as both are polar and charged amino acids, the H631K was also constructed. However, $t_{1/2(65\ ^\circ C)}$ of H631K was worse than that of H631R, especially after multi-point combined mutations (Fig. 4*C*). Therefore, H631R was a better choice for combinatorial mutation.

As shown in Table 2, the accumulation of the four selected mutations clearly showed additive effects on both thermodynamic and kinetic stability. The $t_{1/2(65\ ^\circ C)}$ of the WT, M16 (H631R), M29 (H631R/L382P), M30 (H631R/L382P/S414N) was 22.91, 28.69, 35.93, 45.68, and 52.93 h, respectively. At 70 °C, M31 retained 67% of the enzyme activity after incubation for 90 min, revealing that M31 was undoubtedly the ASase with the best $t_{1/2}$ reported (Fig. 6, *A* and *B*). The optimum temperature of M31 was shifted from 55 to 57.5 °C (Fig. 6*C*), and the specific activity of the purified M31 was 3.09 unit/mg at 57.5 °C. Additionally, M31 showed good temperature tolerance, retaining more than 75% relative activity between 40 °C and 65 °C.

MD simulations were performed at 348 K to understand the stabilizing effect of these mutations. As shown in Fig. S4, M31 showed a lower average RMSD value of 0.3888, while WT showed an average RMSD value of 0.4262, indicating M31 was more stable than WT during the simulations. RMSF value (Fig. 7*A*) also showed that after mutations combined, the flexibility of residues at the subunit interface decreased, in line with the fact that the overall stability of M31 was enhanced. In addition, the average absolute binding-free energy (ΔG_{bind}) between one chain and the other three chains of M31 analyzed by molecular mechanics generalized Born surface area was −82.22 kcal/mol, which was much lower than −72.87 kcal/mol of WT (Fig. 7*B*). Among four mutation sites, H631R contributed the most to the overall relative binding free energy ($\Delta\Delta G_{bind}$) with an average of −6.12 kcal/mol (Fig. 7*C*).

Superior performance of M31 in α-1,4-glucan synthesis

The polymerization reaction is the main reaction catalyzed by ASase when sucrose is the sole substrate (Fig. 1) and can produce amylose-like polymers called α-1,4-glucans. As shown in Figure 6*D*, the optimum temperatures for polymerization activity of M31 were shifted from 45 to 50 °C. Furthermore, the α-glucan-synthesizing ability of M31 was evaluated by using a high concentration of 1 M sucrose as the substrate and reacting at 50 °C for 48 h. As shown in Figure 6, *E* and *F*, under the same reaction conditions, the amount and degree of polymerization of α-1,4-glucan synthesized using mutant M31 as catalyst were higher than those of using WT. Noticeable α-1,4-glucans were detected even when adding 0.04 unit/ml M31 (Fig. 6*E*).

Discussion

Most thermophilic proteins have a higher oligomerization state than their mesophilic homologs, and the intersubunit interaction is considered one of the primary mechanisms for stabilizing thermophilic proteins (22). However, more structural information is still needed to verify this mechanism, especially the quaternary structure assembly information. To date, only a few tetrameric structures of the GH13 family, a large enzyme family, have been reported (Fig. S5), including trehalose synthase (TreS; PDB entry: 4LXF) (23) and glycogen debranching enzyme (TreX; PDB entry: 2VNC) (24). The relationship between intersubunit interactions and their thermostability is also unclear. In this work, we reported the crystal structure of CT-ASase. To our knowledge, this is the first atomic-resolution structure of a tetrameric ASase, and its quaternary structure assembly mode is different from other known structures of GH13 family enzymes. For example, the interface of TreS from *Mycobacterium tuberculosis* (PDB entry: 4LXF) (23) is mediated by the interaction between two β-sandwich domains belonging to two subunits, respectively (Fig. S5*A*). By contrast, the β-sandwich domain of CT-ASase interacted with other domains, such as the domain B', indicating that the quaternary structure of CT-ASase may present another assembly mode of the GH13 family.

Then, based on the structural information, a series of mutations were rationally designed. The results show that constructing new intersubunit interactions to strengthen the relatively weak interface effectively enhanced the thermostability of the CT-ASase. H631R had the highest $\Delta t_{1/2(65\ ^\circ C)}$ among all single-point mutants. Through LigPlot analysis, two new intersubunit hydrogen bonds were formed between Arg631 of chain A (B/C/D) and Glu416 of chain D (C/B/A) and thereby stabilizing the interdimer interface (Fig. 5*B*). The results of MD simulation showed that among the four mutation sites of M31, the change from histidine to arginine at

Table 2
Characteristics of the mutants of CT-ASase with enhanced thermostability

Abbreviation	Mutation	T_m (°C)[a]	$t_{1/2}$ (h)[b]	Relative activity (%)[c]
WT		74.29	22.91	100.0
M16	H631R	74.91	28.69	82.2 ± 1.2
M22	L382P	74.84	25.05	113.6 ± 1.1
M17	S414N	74.79	26.22	109.7 ± 1.6
M27	P618I	74.33	26.31	90.3 ± 0.5
M29	H631R/L382P	75.28	35.93	106.3 ± 1.0
M30	H631R/L382P/S414N	75.98	45.68	104.8 ± 0.8
M31	H631R/L382P/S414N/P618I	76.09	52.93	107.0 ± 0.2

Abbreviation: DSC, differential scanning calorimetry.
[a] These data were estimated using nano-DSC.
[b] These data were the half-life ($t_{1/2}$) at 65 °C.
[c] These data were estimated at 55 °C.

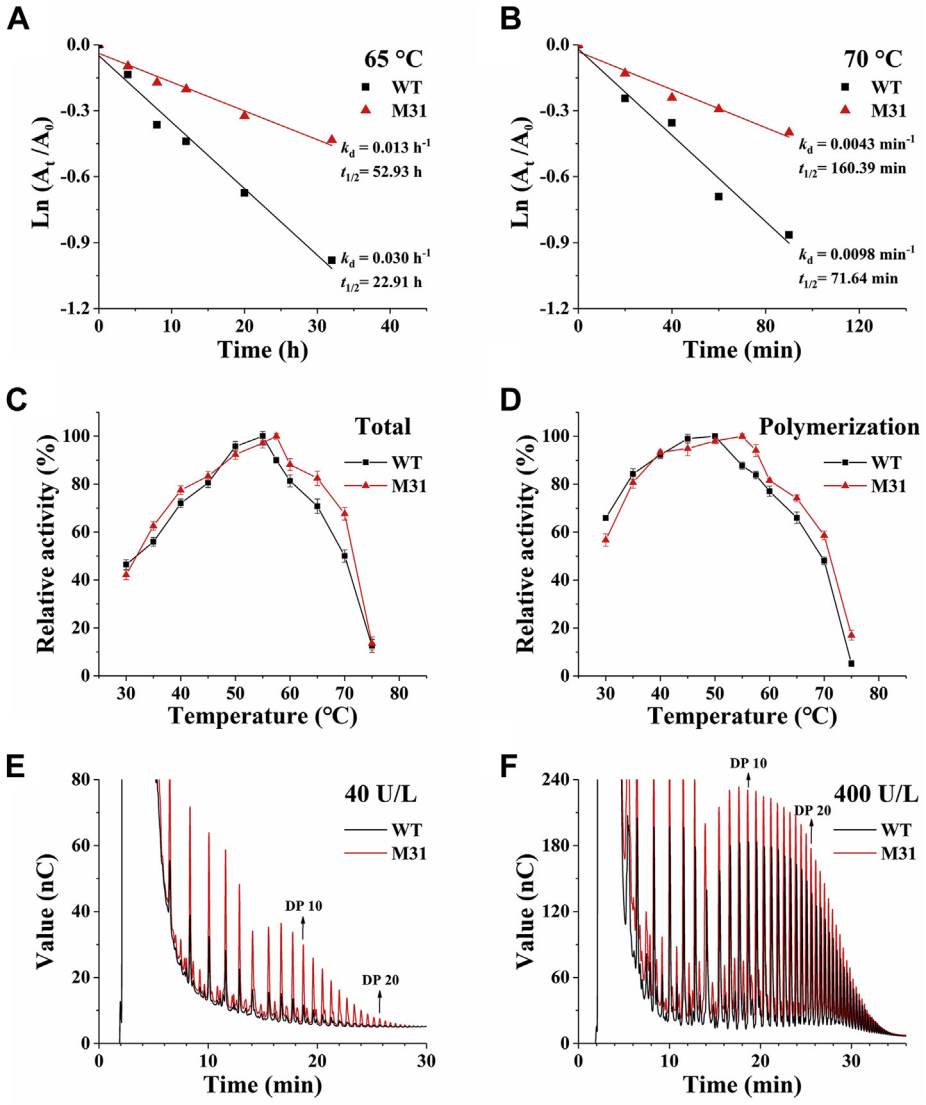

Figure 6. Comparison of the enzymatic properties of the wildtype CT-ASase and M31. The half-life ($t_{1/2}$) at (*A*) 65 °C and (*B*) 70 °C. The activity of CT-ASase and its mutants without any preincubation was defined as A_0. The activity of CT-ASase and its mutants preincubated for a certain time was defined as A_t. The $t_{1/2}$ was obtained by the formula of $t_{1/2} = \ln 2/k_d$, and the k_d (decay constants) was the negative value of the slope of linear fit functions. Effect of temperature on (*C*) total activity and (*D*) polymerization activity. Analysis of the α-glucan produced from sucrose at 50 °C using HPAEC when adding (*E*) 40 U/l and (*F*) 400 U/l enzymes. Since α-glucans with different degrees of polymerization (DP) have different retention times, each peak shown in the figure represented α-glucans with different DP. CT-ASase, amylosucrase from *Calidithermus timidus* DSM 17022; HPAEC, high-performance anion-exchange chromatography.

position 631 contributed the most, accounting for 65.2% of the total $\Delta\Delta G_{bind}$, and indicated that the two new hydrogen bonds had brought the chain A/B closer to the chain D/C (Fig. 7*C* and Data S1). Considering that in the wildtype, the average buried area of the intradimer interface was about twice that of the interdimer interface, it is reasonable that strengthening the interaction network of the relatively weak interdimer interface can have a considerable impact on thermostability.

To date, there are no reports on protein engineering of the thermostability of multimeric ASases. Several studies have reported engineering of monomeric NP-ASase and their enhancement of thermostability benefited from reshaping the active site (25), reorganizing intramolecular salt bridges, or introducing new hydrogen bond interactions (26–29). However, these mutants of NP-ASase are only more stable at 50 °C (Table S4), and their thermostability is much lower than that of some wildtype multimeric ASases, such as CT-ASase. In comparison, M31, which possessed a half-life of 52.93 h at 65 °C, is undoubtedly a hyperstable catalyst with the potential to be used in various applications limited by thermostability.

In order to explore the possible applications of M31, its polymerization ability at 50 °C was proved in this study. Amylose-like polymers can be used to prepare biodegradable plastic substitutes with low oxygen diffusion, high transparency and flexibility, functional foods with lower risk of diabetes and obesity, and sustained-release drug delivery system (30–33). Since it is difficult and costly to completely separate amylose and amylopectin from plant starch, enzymatic approaches have been considered an alternative way to synthesize amylose. However, enzymatic approaches are also

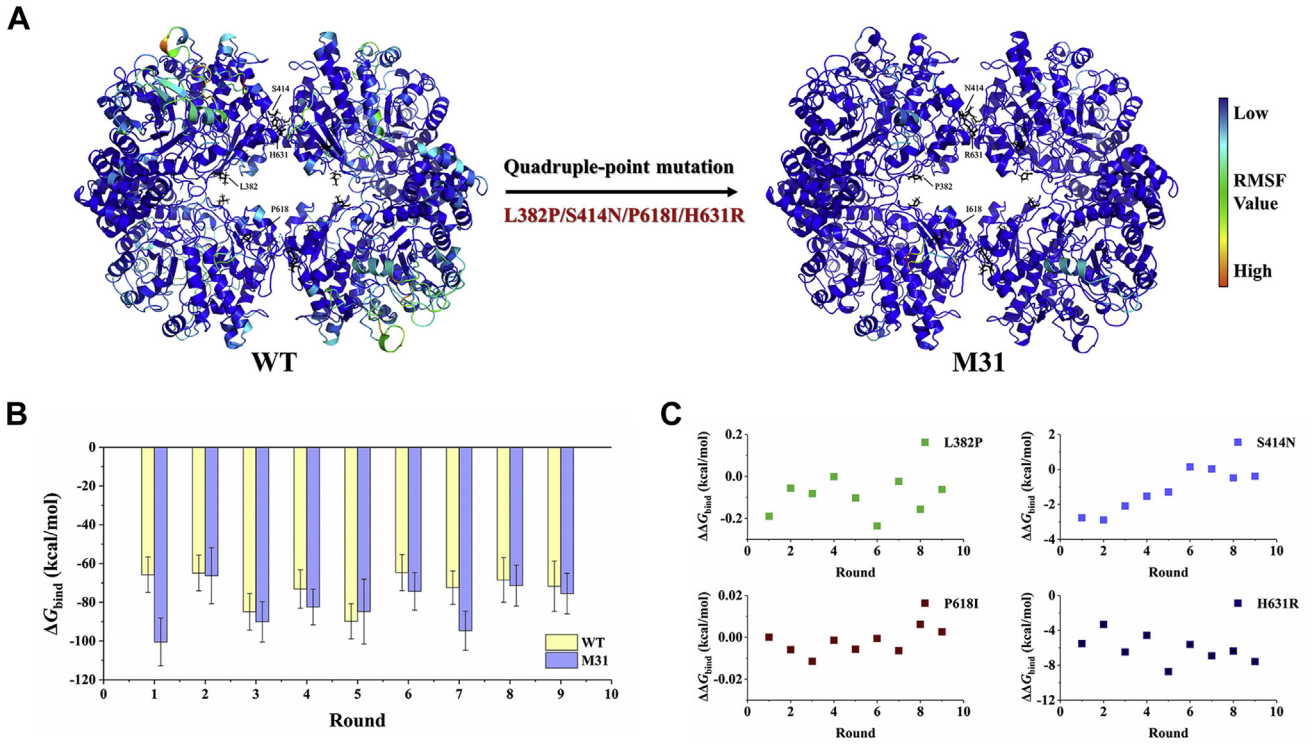

Figure 7. Comparison of the WT and M31 using MD simulation. *A*, graphical representation of RMSF values. The color of the secondary structure is displayed from *red* to *blue*, corresponding to the relative RMSF value of each residue from high to low. The four mutated residues on each subunit were shown as *black sticks* to illustrate better the location of these mutation sites on the protein. *B*, comparison of ΔG_{bind} of the WT and M31 calculated by MM/GBSA. Error bars correspond to standard deviation. *C*, stabilizing effect of each mutated site. The $\Delta\Delta G_{bind}$ was obtained by subtracting the ΔG_{bind} of WT from the ΔG_{bind} of M31. All ΔG_{bind} were calculated for nine independent rounds, and all MD simulations were performed at 348 K. CT-ASase, amylosucrase from *Calidithermus timidus* DSM 17022; ΔΔGbind, the relative binding free energy; MD, molecular dynamics; MM/GBSA, molecular mechanics generalized Born surface area; RMSF, root mean square fluctuation.

hampered by the poor thermostability of the catalysts. Therefore, it is meaningful to investigate the glucans synthesizing ability of M31. As shown in Figure 6*D*, the optimum temperatures for polymerization activity of M31 shifted from 45 to 50 °C, which can increase the solubility and decrease the viscosity of the products. As shown in Figure 6*E*, detectable amylose-like polymers were produced at 50 °C when adding a trace amount of M31. By contrast, most ASases are inactive or cannot produce detectable polymerization products at this temperature (13). Considering that the amylose-converting enzymes usually have an optimum temperature of about 50 °C, M31 has the potential to be used in a multienzyme cascade reaction together with the amylose-converting enzymes to produce functional carbohydrates from the cheap substrate sucrose.

Furthermore, the workflow employed here presents a feasible way to enhance the thermostability of protein, especially multimeric protein. In this work, five common strategies of rational design were adopted. The candidate mutations with higher scores in each strategy and the candidate mutations at the intersection of each strategy were selected for biochemical verification. Surprisingly, mutations that displayed enhanced T_m values were all located on the subunit interface or on the surface close to the interface, which also verifies that the thermostability of tetrameric CT-ASase is closely related to its interface stability. Perhaps because these mutation sites were selected by multiple strategies and were located far from the active sites, the quadruple-point mutant M31 possessed fully retained enzyme activity. However, more work is needed to verify the relationship between multiple strategy selection and enzyme activity retention. In addition, it will be interesting to improve this workflow with the help of computational-aided design and try to use it to improve other enzymes' thermal stability. Furthermore, other possible applications of CT-ASase limited by thermostability also need to be investigated.

In conclusion, this study reported the first crystal structure of tetrameric ASase, which presented a novel quaternary organization among GH13 family enzymes and confirmed the importance of interface regions for thermostability. Five strategies, including interface engineering, folding energy calculations, consensus sequence, hydrophobic effects enhancement, and B-factor analysis, were combined in a workflow and applied to enhance the thermostability of CT-ASase. A quadruple-point mutant, M31, with greatly improved thermostability and α-glucan-synthesizing ability, was obtained through limited efforts. M31 is undoubtedly a robust catalyst with the potential to be used in various applications limited by thermostability. Our results pave the way for the construction of protein stabilization strategies that combine structural and evolutionary approaches and provide information for optimizing the computational workflows for

protein engineering. The effective and minimally invasive strategy adopted here may also be a potential option for systematically enhancing the thermostability of multimeric enzymes.

Experimental procedures

Expression and purification

Expression and purification of recombinant CT-ASase and its variants were conducted as described in a previous study (14). The gene encoding CT-ASase and its variants were fused with the sequence encoding a 6× histidine tag at the 3'-terminus and cloned into a pET-22b (+) vector. These 6-histidine tag–fused proteins were overexpressed in *Escherichia coli* BL21(DE3) and purified by affinity chromatography using a HisTrap HP column (GE Healthcare). To meet the requirement of crystallization, the CT-ASase eluted in the previous step was further purified by size-exclusion chromatography using a HiLoad 16/600 Superdex 200 prep grade column (GE Healthcare). Tris-HCl buffer (25 mM) containing 150 mM NaCl was used as the mobile phase at a 1 ml/min flow rate. Finally, the peak fractions collected in the previous step were concentrated to 10 mg/ml using an Amicon Ultra centrifugal filter unit (Merck Millipore Ltd). Unless otherwise stated, the pH of all the buffers was 7.0.

Crystallization, data collection, and structure determination

We performed robotized crystallization trials (STP Labtech) by mixing 0.8 μl 10 mg/ml protein solution with an equal volume of reservoir solutions and then equilibrating the mixture with an 80 μl reservoir solution. Commercial kits were used as the initial screening conditions, and 96-well sitting drop plates were used for crystal growth at 291 K. Diffraction-quality crystals of CT-ASase were obtained after 2 weeks from PEGRx HT (Hampton Research Corp) condition H8 (0.2 M ammonium acetate, 0.1 M Tris pH 8.0, and 16% w/v polyethylene glycol 10,000). Then, crystals of CT-ASase were transferred to a cryoprotectant solution, which consisted of a crystallization condition solution supplemented with 25% (v/v) glycerol, and quickly cooled in liquid nitrogen.

Datasets were collected at the BL19U1 synchrotron radiation beamline of Shanghai Synchrotron Radiation Facility (SSRF) at 100 K and were processed and scaled with HKL-2000 (34). After that, the molecular replacement was performed using the MOLREP (35) program from the CCP4 package (36). It used the structure of DG-ASase (PDB entry: 3UCQ) (17) as the model to determine the structure of CT-ASase. Further refinement of the structure was conducted using the REFMAC5 (37) program from the CCP4 package, alternated with cycles of manual reconstruction in the electron density maps using Coot (38). Water molecules were automatically added using Coot and manually checked. The ligand molecules were manually added using Coot in residual maps. In addition, all graphical presentations of the structure were performed using PyMOL.

Computational design

The three-dimensional structure of WT obtained from X-ray diffraction was used in the computational design. At first, a systematic analysis of the crystal structure of CT-ASase was conducted to find the subunit interface residues using PISA (39) and LigPlot+ (40). The residues that contribute negligibly to the buried area of the interface and the highly conserved residues in the consensus sequence were discarded. Second, the FireProt (41) web server, which integrated methods including FoldX and Rosetta, was used to calculate the free energy of folding ($\Delta\Delta G_{fold}$) and automatically design some thermostable mutants. Then, $Rosetta_{VIP}$ (42) (void identification and packing), an automated protocol within the RosettaDesign framework, was used to redesign the WT to get a well-packed conformation. Three iterations were run, and the detailed protocol is available at https://www.rosettacommons.org/demos/latest/public/vip/README. Next, Consensus Finder (43) was used to find evolution-based candidates. Finally, B-FITTER (44) was used to extract and rank the residues' B-factor and then sort out the high B-factor residues among the candidates selected by the previous strategies.

Site-directed mutagenesis

Mutations of CT-ASase were accomplished by a one-step PCR method using the primers and templates listed in Table S5, and the products were sequenced by GENEWIZ Inc. The PCR system (20 μl) composed 10 μl 2× PrimerSTAR MAX DNA Polymerase (Takara Bio Inc), 10 ng template, 5 pmol forward and reverse primers, and double-distilled water. The PCR program was as follows: 1 cycle at 95 °C for 3 min; 32 cycles at 95 °C for 30 s, 56 °C for 30 s, and 72 °C for 3 min 45 s; 1 cycle at 72 °C for 5 min; and 4 °C for storage. Except for M7, M8, and M32, other amplified PCR products were digested with *Dpn*I (Takara Bio Inc) at 37 °C for 1.5 h and transformed into *E. coli* JM109. The seamless cloning method was used to construct plasmids expressing M7, M8, and M32. The linearized vector and DNA fragment, prepared by PCR as described above, were assembled using Seamless Cloning Master Mix (Sangon Biotech Co, Ltd) at 50 °C for 20 min and transformed into *E. coli* JM109.

Activity and biochemical properties assay

Unless otherwise stated, the activity of recombinant CT-ASase and its variants was determined using 0.1 M sucrose as a substrate at 55 °C and pH 7.0 (50 mM sodium phosphate buffer) for 30 min. The reaction was terminated by heating at 95 °C for 15 min. Monosaccharides and disaccharides were analyzed using a high-performance liquid chromatography system equipped with a Sugar-Pak I column and a refractive index detector (Waters Corporation). Ultrapure water containing 50 mg/l EDTA calcium disodium was used as the mobile phase, running at 85 °C with a flow rate of 0.4 ml/min. The amount of enzyme that catalyzed the release of 1 μmol of fructose per min was defined as one unit of total activity. The amount of enzyme that catalyzed the release of 1 μmol of

glucose per min was defined as one unit of hydrolysis activity. The polymerization activity was defined as the total activity minus the hydrolysis activity. In addition, polysaccharides were analyzed using a high-performance anion-exchange chromatography system equipped with a Dionex CarboPac PA200 column and pulsed amperometric detection (Thermo Fisher Scientific). Buffers A, B, and C were 200 mM NaOH, 1 M sodium acetate, and ultrapure water. Samples were diluted ten times and eluted with a linear gradient of 4% to 40% buffer B and 46% to 10% buffer C. The elution time was 40 min, and the flow rate was 0.5 ml/min.

The thermal shift (ΔT_m) between recombinant CT-ASase and its variants was preliminarily screened by DSF using SYPRO orange protein gel stain and C1000 Touch thermal cycler (Bio-Rad). Samples containing 5 mg/ml protein were heated from 25 to 100 °C at a heating rate of 1 °C/min, and the data were analyzed using CFX Manager and DMAN software. After preliminary screening by DSF, nano-differential scanning calorimetry was used to accurately determine the T_m value of mutants using the same method as described in the previous study (14). To investigate kinetic stability, CT-ASase and its variants were preincubated without substrate at 65 and 70 °C. Then, the protein samples were taken at certain time intervals, and their activity was determined using the assay method (0.1 M sucrose, pH 7.0, 55 °C, and 30 min). The effect of temperature on the activity of CT-ASase and M31 was compared using 0.1 M sucrose at 30 to 75 °C and pH 7.0 (50 mM sodium phosphate buffer) for 30 min. The α-glucan-synthesizing ability of CT-ASase and M31 was compared using 1 M sucrose at 50 °C and pH 7.0 (50 mM sodium phosphate buffer) for 48 h. Unless otherwise stated, all experiments were repeated thrice.

MD simulations

Three independent 5-ns constant pressure equilibration simulations (NPT) were executed in the GROMACS program, and then the analytical tools in the GROMACS package were used to calculate RMSD and RMSF. Nine 2-ns independent NPT simulations were conducted (18 ns total simulation time) to get the binding free energies using AMBER18. MMPBSA.py python script in AMBER18 suite was used for calculating binding free energy. The configurational sampling was taken every 5 ps from the last 1 ns trajectories of each simulation. All molecular dynamics simulations were performed at 348 K.

Data availability

The atomic coordinate of the CT-ASase was deposited in the PDB under the PDB entry 7ESH. All other data are available in the main text or the supporting information.

Supporting information—This article contains supporting information (14, 25–29).

Acknowledgments—We thank the staffs of beamline BL18U1 and BL19U1 of Shanghai Synchrotron Radiation Facility for assistance during X-ray data collection.

Author contributions—Y. T., X. H., D. N., W. X., C. G., W. Z., Q. C., Y. R., and W. M. conceptualization; Y. T., X. H., and D. N. investigation; Y. T. writing-original draft; X. H. data curation; W. X., C. G., and W. Z. formal analysis; Q. C. software; Y. R. and W. M. supervision; Y. R. and W. M. writing-review & editing.

Funding and additional information—This work was supported by the National Natural Science Foundation of China (No. 31922073) and the Natural Science Foundation of Jiangsu Province (No. BK20180607 and BK20202002).

Conflict of interest—The authors declare that they have no conflicts of interest with the contents of this article.

Abbreviations—The abbreviations used are: ASase, amylosucrase; CT-ASase, amylosucrase from *Calidithermus timidus* DSM 17022; DG-ASase, amylosucrase from *Deinococcus geothermalis*; DRd-ASase, amylosucrase from *Deinococcus radiodurans*; DSF, differential scanning fluorimetry; ΔG_{bind}, the absolute binding free energy; $\Delta\Delta G_{bind}$, the relative binding free energy; GH, glycoside hydrolases; k_d, decay constants; MD, molecular dynamics; MM/GBSA, molecular mechanics generalized Born surface area; PDB, Protein Data Bank; RMSD, root mean square deviation; RMSF, root mean square fluctuation; $t_{1/2}$, half-life; WT, wildtype CT-ASase.

References

1. Robinson, P. K. (2015) Enzymes: principles and biotechnological applications. *Essays Biochem.* **59**, 1–41
2. Yeoman, C. J., Han, Y., Dodd, D., Schroeder, C. M., Mackie, R. I., and Cann, I. K. (2010) Thermostable enzymes as biocatalysts in the biofuel industry. *Adv. Appl. Microbiol.* **70**, 1–55
3. Ibrahim, N. E., and Ma, K. (2017) Industrial applications of thermostable enzymes from extremophilic microorganisms. *Curr. Biochem. Eng.* **4**, 75–98
4. Markova, K., Chmelova, K., Marques, S. M., Carpentier, P., Bednar, D., Damborsky, J., *et al.* (2020) Decoding the intricate network of molecular interactions of a hyperstable engineered biocatalyst. *Chem. Sci.* **11**, 11162–11178
5. Sun, Z., Liu, Q., Qu, G., Feng, Y., and Reetz, M. T. (2019) Utility of B-factors in protein science: interpreting rigidity, flexibility, and internal motion and engineering thermostability. *Chem. Rev.* **119**, 1626–1665
6. Meng, Q., Capra, N., Palacio, C. M., Lanfranchi, E., Otzen, M., van Schie, L. Z., *et al.* (2020) Robust ω-transaminases by computational stabilization of the subunit interface. *ACS Catal.* **10**, 2915–2928
7. Pace, C. N., Fu, H., Fryar, K. L., Landua, J., Trevino, S. R., Shirley, B. A., *et al.* (2011) Contribution of hydrophobic interactions to protein stability. *J. Mol. Biol.* **408**, 514–528
8. Kuhlman, B., and Bradley, P. (2019) Advances in protein structure prediction and design. *Nat. Rev. Mol. Cell Biol.* **20**, 681–697
9. Goldenzweig, A., and Fleishman, S. J. (2018) Principles of protein stability and their application in computational design. *Annu. Rev. Biochem.* **87**, 105–129
10. Lombard, V., Golaconda Ramulu, H., Drula, E., Coutinho, P. M., and Henrissat, B. (2014) The carbohydrate-active enzymes database (CAZy) in 2013. *Nucleic Acids Res.* **42**, D490–D495
11. Tian, Y., Chen, Q., and Zhang, W. (2021) Amylosucrase: a versatile sucrose-utilizing transglucosylase for glycodiversification. In: Mu, W., Zhang, W., Chen, Q., eds. *Novel Enzymes for Functional Carbohydrates Production: From Scientific Research to Application in Health Food Industry*, Springer Singapore, Singapore: 223–249
12. Moulis, C., Andre, I., and Remaud-Simeon, M. (2016) GH13 amylosucrases and GH70 branching sucrases, atypical enzymes in their respective families. *Cell. Mol. Life Sci.* **73**, 2661–2679
13. Tian, Y., Xu, W., Zhang, W., Zhang, T., Guang, C., and Mu, W. (2018) Amylosucrase as a transglucosylation tool: from molecular features to bioengineering applications. *Biotechnol. Adv.* **36**, 1540–1552

14. Tian, Y., Xu, W., Guang, C., Zhang, W., and Mu, W. (2019) Thermostable amylosucrase from *Calidithermus timidus* DSM 17022: insight into its characteristics and tetrameric conformation. *J. Agric. Food Chem.* **67**, 9868–9876
15. Stam, M. R., Danchin, E. G. J., Rancurel, C., Coutinho, P. M., and Henrissat, B. (2006) Dividing the large glycoside hydrolase family 13 into subfamilies: towards improved functional annotations of α-amylase-related proteins. *Protein Eng. Des. Sel.* **19**, 555–562
16. Skov, L. K., Mirza, O., Sprogoe, D., Dar, I., Remaud-Simeon, M., Albenne, C., *et al.* (2002) Oligosaccharide and sucrose complexes of amylosucrase - structural implications for the polymerase activity. *J. Biol. Chem.* **277**, 47741–47747
17. Guerin, F., Barbe, S., Pizzut-Serin, S., Potocki-Veronese, G., Guieysse, D., Guillet, V., *et al.* (2012) Structural investigation of the thermostability and product specificity of amylosucrase from the bacterium Deinococcus geothermalis. *J. Biol. Chem.* **287**, 6642–6654
18. Bosshart, A., Panke, S., and Bechtold, M. (2013) Systematic optimization of interface interactions increases the thermostability of a multimeric enzyme. *Angew. Chem. Int. Ed. Engl.* **52**, 9673–9676
19. Lee, B. K., and Richards, F. M. (1971) The interpretation of protein structures: estimation of static accessibility. *J. Mol. Biol.* **55**, 379–400
20. Richards, F. M. (1977) Areas, volumes, packing, and protein structure. *Annu. Rev. Biophys. Bioeng.* **6**, 151–176
21. Ponder, J. W., and Richards, F. M. (1987) Tertiary templates for proteins. Use of packing criteria in the enumeration of allowed sequences for different structural classes. *J. Mol. Biol.* **193**, 775–791
22. Vieille, C., and Zeikus, G. J. (2001) Hyperthermophilic enzymes: sources, uses, and molecular mechanisms for thermostability. *Microbiol. Mol. Biol. Rev.* **65**, 1–43
23. Roy, R., Usha, V., Kermani, A., Scott, D. J., Hyde, E. I., Besra, G. S., *et al.* (2013) Synthesis of α-glucan in mycobacteria involves a hetero-octameric complex of trehalose synthase TreS and maltokinase Pep2. *ACS Chem. Biol.* **8**, 2245–2255
24. Woo, E. J., Lee, S., Cha, H., Park, J. T., Yoon, S. M., Song, H. N., *et al.* (2008) Structural insight into the bifunctional mechanism of the glycogen-debranching enzyme TreX from the Archaeon Sulfolobus solfataricus. *J. Biol. Chem.* **283**, 28641–28648
25. Daudé, D., Topham, C. M., Remaud-Simeon, M., and Andre, I. (2013) Probing impact of active site residue mutations on stability and activity of Neisseria polysaccharea amylosucrase. *Protein Sci.* **22**, 1754–1765
26. van der Veen, B. A., Skov, L. K., Potocki-Veronese, G., Gajhede, M., Monsan, P., and Remaud-Simeon, M. (2006) Increased amylosucrase activity and specificity, and identification of regions important for activity, specificity and stability through molecular evolution. *FEBS J.* **273**, 673–681
27. Emond, S., Potocki-Veronese, G., Mondon, P., Bouayadi, K., Kharrat, H., Monsan, P., *et al.* (2007) Optimized and automated protocols for high-throughput screening of amylosucrase libraries. *J. Biomol. Screen.* **12**, 715–723
28. Emond, S., Andre, I., Jaziri, K., Potocki-Veronese, G., Mondon, P., Bouayadi, K., *et al.* (2008) Combinatorial engineering to enhance thermostability of amylosucrase. *Protein Sci.* **17**, 967–976
29. Daudé, D., Vergès, A., Cambon, E., Emond, S., Tranier, S., André, I., *et al.* (2019) Neutral genetic drift-based engineering of a sucrose-utilizing enzyme toward glycodiversification. *ACS Catal.* **9**, 1241–1252
30. Qi, P., You, C., and Zhang, Y. H. P. (2014) One-pot enzymatic conversion of sucrose to synthetic amylose by using enzyme cascades. *ACS Catal.* **4**, 1311–1317
31. Seung, D. (2020) Amylose in starch: towards an understanding of biosynthesis, structure and function. *New Phytol.* **228**, 1490–1504
32. Obiro, W. C., Sinha Ray, S., and Emmambux, M. N. (2012) V-amylose structural characteristics, methods of preparation, significance, and potential applications. *Food Rev. Int.* **28**, 412–438
33. Nishimura, T., and Akiyoshi, K. (2017) Amylose engineering: phosphorylase-catalyzed polymerization of functional saccharide primers for glycobiomaterials. *Wiley Interdiscip. Rev. Nanomed. Nanobiotechnol.* **9**, e1423
34. Minor, W., Cymborowski, M., Otwinowski, Z., and Chruszcz, M. (2006) HKL-3000: the integration of data reduction and structure solution - from diffraction images to an initial model in minutes. *Acta Crystallogr. D Biol. Crystallogr.* **62**, 859–866
35. Vagin, A., and Teplyakov, A. (2010) Molecular replacement with MOLREP. *Acta Crystallogr. D Biol. Crystallogr.* **66**, 22–25
36. Winn, M., Ballard, C. C., Cowtan, K. D., Dodson, E. J., and Wilson, K. S. (2011) Overview of the CCP4 suite and current development. *Acta Crystallogr. D Biol. Crystallogr.* **67**, 235–242
37. Murshudov, G. N., Skubák, P., Lebedev, A. A., Pannu, N. S., Steiner, R. A., Nicholls, R. A., *et al.* (2011) REFMAC5 for the refinement of macromolecular crystal structures. *Acta Crystallogr. D Biol. Crystallogr.* **67**, 355–367
38. Emsley, P., and Cowtan, K. (2004) Coot: model-building tools for molecular graphics. *Acta Crystallogr. D Biol. Crystallogr.* **60**, 2126–2132
39. Krissinel, E., and Henrick, K. (2007) Inference of macromolecular assemblies from crystalline state. *J. Mol. Biol.* **372**, 774–797
40. Laskowski, R. A., and Swindells, M. B. (2011) LigPlot+: multiple ligand-protein interaction diagrams for drug discovery. *J. Chem. Inf. Model.* **51**, 2778–2786
41. Musil, M., Stourac, J., Bendl, J., Brezovsky, J., Prokop, Z., Zendulka, J., *et al.* (2017) FireProt: web server for automated design of thermostable proteins. *Nucleic Acids Res.* **45**, W393–W399
42. Borgo, B., and Havranek, J. J. (2012) Automated selection of stabilizing mutations in designed and natural proteins. *Proc. Natl. Acad. Sci. U. S. A.* **109**, 1494–1499
43. Jones, B. J., Kan, C. N. E., Luo, C., and Kazlauskas, R. J. (2020) Chapter six - consensus finder web tool to predict stabilizing substitutions in proteins. In: Tawfik, D. S., ed. *Methods in Enzymology*, Academic Press, Cambridge, MA: 129–148
44. Reetz, M. T., and Carballeira, J. D. (2007) Iterative saturation mutagenesis (ISM) for rapid directed evolution of functional enzymes. *Nat. Protoc.* **2**, 891–903